Direct quantification of sinking velocities across unicellular algae

Teemu P. Miettinen*[,1,#], Annika L. Gomez*[,2], Yanqi Wu*[,1], Weida Wu[1,3], Thomas R. Usherwood[1,4], Benjamin R.K. Roller[5], Martin F. Polz[5,#], and Scott R. Manalis[1,3,6,#]

Affiliations:
[1] Koch Institute for Integrative Cancer Research, Massachusetts Institute of Technology, Cambridge, MA 02139, USA.
[2] Department of Civil and Environmental Engineering, Massachusetts Institute of Technology, Cambridge, MA 02139, USA.
[3] Department of Biological Engineering, Massachusetts Institute of Technology, Cambridge, MA 02139, USA.
[4] Harvard-MIT Department of Health Sciences and Technology, Institute for Medical Engineering and Science, Massachusetts Institute of Technology, Cambridge, MA 02139, USA.
[5] Division of Microbial Ecology, Centre for Microbiology and Environmental Systems Science, University of Vienna, Vienna, 1030, Austria.
[6] Department of Mechanical Engineering, Massachusetts Institute of Technology, Cambridge, MA 02139, USA.

* These authors contributed equally to this work
[#] Correspondence to: teemu@mit.edu & martin.f.polz@univie.ac.at & srm@mit.edu

Keywords: Algae, phytoplankton, cell size, Stokes' law, sinking velocity

ABSTRACT

Eukaryotic phytoplankton, also known as algae, form the basis of marine food webs and are responsible for most of marine carbon sequestration when their dead biomass sinks to the ocean floor. Living algae must regulate their vertical movement in the ocean to balance access to light at the surface and nutrients in deeper layers. This can be achieved by motility, as in most green algae, or by changing cell size and composition, as in non-motile species like diatoms. However, motility-independent sinking velocities, as defined by Stokes' law remain largely unknown, and it is unclear if motile species also adjust their cell size and composition in response to environmental changes. Here, we directly quantify single-cell mass and volume to calculate sinking velocity according to Stokes' law in diverse clades of unicellular marine microalgae under different nutrient conditions. We find species vary in cell density by >10% and in volume by >3000%, resulting in sinking velocities that range from 0.2 to 12.8 µm/s. We observe examples of motile dinoflagellate and green algal species where nutrient limitation causes cells to increase their sinking velocity by changing cell mass rather than volume, while a diatom species did not respond to nutrient limitation. We also find that single-cell sinking velocities display significant intraspecies heterogeneity, but only ~50% of this heterogeneity is accounted for by variation in cell volume. Overall, our work reveals unexpected biophysical responses to nutrient limitation in motile algae and provides an approach for direct sinking velocity measurements for estimations of carbon fluxes in the oceans.

MAIN TEXT

Algae are a genetically, morphologically, and biophysically diverse group of photosynthetic microorganisms. Algae comprise the base of the marine food webs and are responsible for approximately 75-90% of marine carbon fixation by mass (1). Consequently, the sinking of dead algal cells is the main contributor to the 'biological pump', which sequesters carbon dioxide from the atmosphere to deep oceans and marine sediments. Hence a quantitative understanding of sinking velocities of different algae is needed for modeling marine ecosystems and carbon fluxes, especially in the context of global change (2–6).

The vertical movement of live cells impacts their growth, viability, and community composition, as both organic and inorganic nutrients are more abundant deeper in the ocean while light is stronger at the surface. Hence algae can benefit from differential positioning in the water column depending on whether they are limited by nutrients or light. Vertical movement is driven by motility, surrounding fluid movement, and gravity-induced sinking. Most algae are motile and migrate in search of light and nutrients. However, some algae, such as diatoms, lack active motility and may adjust their sinking solely by regulating cell size and composition (7–10). Whether motile algal species also adjust their sinking velocities by regulating cell size and composition remains unclear, as live cell sinking and sedimentation rate measurements cannot decouple motility-dependent and independent sinking. Consequently, most studies on gravitational sinking have focused on non-motile species.

In the absence of motility, cell sinking velocity due to gravity depends on the cell's volume and density and drag force from seawater. For spherical cells, this can be derived from Stokes' law (2, 7, 8):

$$V_s = \frac{2(\rho_{cell} - \rho_{fluid})gr^2}{9\mu} \quad (1)$$

where ρ_{cell} is the density of the cell, ρ_{fluid} is the density of the surrounding fluid, g is the gravitational acceleration, r is radius of the cell, and μ is the dynamic viscosity of the fluid. A cell dimension-dependent correction factor can be applied to *Eq(1)* for non-spherical particles (8, 9).

This approach has been widely used to estimate sinking velocities from microscopy-based observations of cell radius, but cell density is rarely known, especially for single cells. We reasoned that independent measurements of cell volume and buoyant mass could be used to calculate sinking velocity without assumptions about cell density (Fig 1A). Buoyant mass, m_b, is defined as

$$m_b = V(\rho_{cell} - \rho_{fluid}) \tag{2}$$

where, V is the volume of the cell. As the fluid density is typically known, cell density, and consequently sinking velocity, can be solved with the knowledge of buoyant mass and volume. Here, we obtain direct measurements of single-cell volumes and buoyant masses to define algae sinking velocities across species and nutrient conditions, revealing examples of motile species that regulate their cell mass to increase sinking velocity upon nutrient depletion.

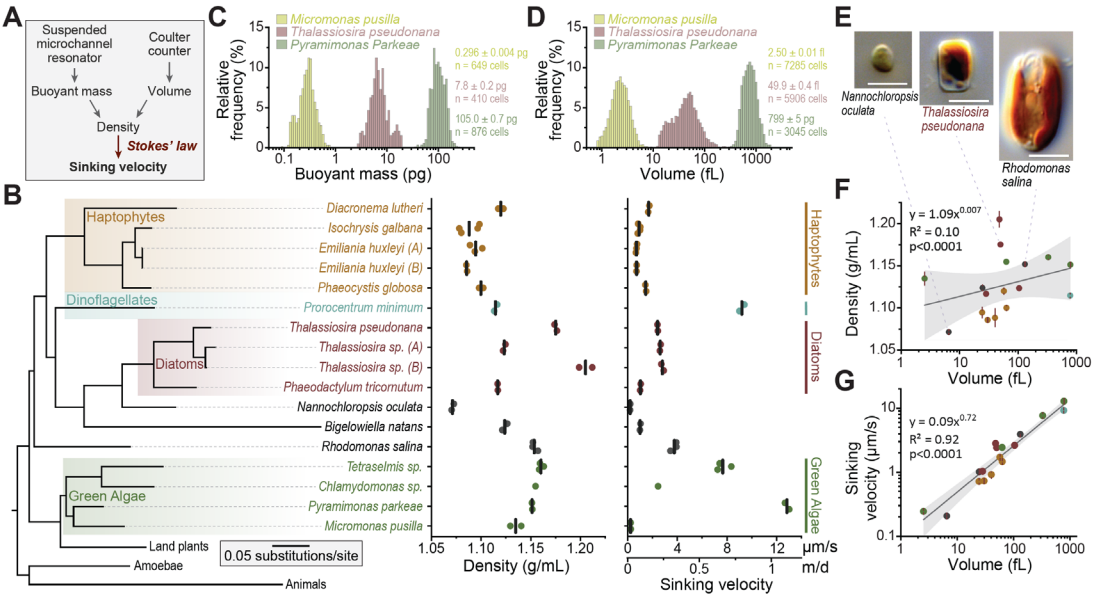

Figure 1. Cell densities and sinking velocities across phylogenetically diverse algae species.
(A) Schematic of the workflow. **(B)** *Left*, a phylogenetic tree of the measured algae species according to 18S rRNA. Animals, amoebae, and land plants are shown for reference. The major clades of algae are color coded. *Right*, cell density and sinking velocity for each species. Dots depict independent experiments and vertical lines depict mean. **(C-D)** Single-cell buoyant mass (C) and volume (D) histograms for three representative species. Mean±SEM and the number of cells measured (n) are indicated. **(E)** Representative images of 3 species studied. Scales bars denote 5 μm. **(F)** Correlation between cell density and volume across species. Dots and error bars depict mean±SD for each species. Species are color coded according to their major clade. **(G)** Same as (F), but the correlation is between sinking velocity and volume.
In (F) and (G), p-values for power law fits were obtained by ANOVA.

RESULTS

We sought to understand the range of sinking velocities across algal species. We characterized cell sinking velocities in unicellular eukaryotic algal species spanning all major clades of algae, including haptophytes, dinoflagellates, diatoms, and green algae (Fig 1B, *left*). In total, we studied 17 species, all of which were verified using 18S rRNA gene sequencing and grown under autotrophic conditions in ambient light and high nutrient L1 or L1-Si media. Single-cell volumes were measured using a Coulter counter, and single-

cell buoyant masses using a suspended microchannel resonator (SMR) (10–12). For a typical sample, we measured the buoyant mass of >300 cells and volume of >4000 cells, resulting in <2% errors in our estimations of population mean buoyant masses and volumes (Figs 1C&D). Overall, the measured algae species spanned ~2.5 orders of magnitude in mass and volume from the ~2.5 fL green alga *Micromonas pusilla* to the ~785 fL green alga *Pyramimonas parkeae* (Fig 1D, Supplemental datasets S1&S2).

Using buoyant mass and volume data, we calculated cell density, which reflects cell water content and molecular composition, for each algal species measured (Fig 1B). Cell densities ranged ~12% between the measured species, from 1.07 g/mL in the small eustigmatophyte *Nannochloropsis oculata* to 1.21 g/mL in a small diatom *Thalassiosira sp.* which was isolated from coastal seawater (isolate B). Curiously, a second diatom isolate (A) that was also identified as *Thalassiosira sp.* displayed significantly lower density. We then calculated the sinking velocities for each species according to *Eq(1)* (Fig 1B). Sinking velocities displayed a wide range, from 0.2 µm/s in *Nannochloropsis oculata* to 12.8 µm/s in *Pyramimonas parkeae*. We also imaged the species studied (Fig 1E) to examine shape-dependency of the sinking velocities. As the highly elongated diatom *Phaeodactylum tricornutum* was the only species where sinking velocities were influenced >5% by cell shape (Supplemental dataset S3), all sinking velocities reported in figures are assuming a spherical object. Overall, genetic relatedness did not predict cell density or sinking velocity. Thus, our results highlight the need to examine the biophysical properties of each species individually.

We next examined the volume dependency of cell density and sinking velocities across species. Cell volumes displayed a weak but statistically significant positive correlation with cell densities (R^2=0.10, Fig 1F). Because density variability is small in comparison to volume variability across species, cell volumes displayed a strong correlation with sinking velocities (R^2=0.92, Fig 1G). Overall, sinking velocities scaled with cell volumes with a scaling exponent of 0.72 ± 0.05 (mean ± SE).

We then compared the biophysical properties of selected algae species under standard culture conditions ("high nutrient", L1 media) and following 5-day culture in nutrient depleted media ("low nutrient", L1/100 media), where nutrient conditions resemble those seen in coastal seawater. We selected four phylogenetically distinct species for investigation: chlorarachniophyte *Bigelowiella natans*, diatom *Phaeodactylum traceroute*, green alga *Tetraselmis sp.*, and dinoflagellate *Prorocentrum minimum*. All species differed in their nutrient responses, with most radical responses observed in *Tetraselmis sp.* (Fig 2A, Supplemental datasets S4-S7), which entered a stationary growth phase under low nutrient but not under high nutrient conditions. *Bigelowiella natans* did not display any nutrient responses, *Phaeodactylum tricornutum* decreased its mass and volume upon a shift to low nutrients, while *Tetraselmis sp.* and *Prorocentrum minimum* both increased their masses upon a shift to low nutrients while maintaining nearly constant volume (Fig 2B). Curiously, in all species with nutrient-dependent responses, buoyant mass

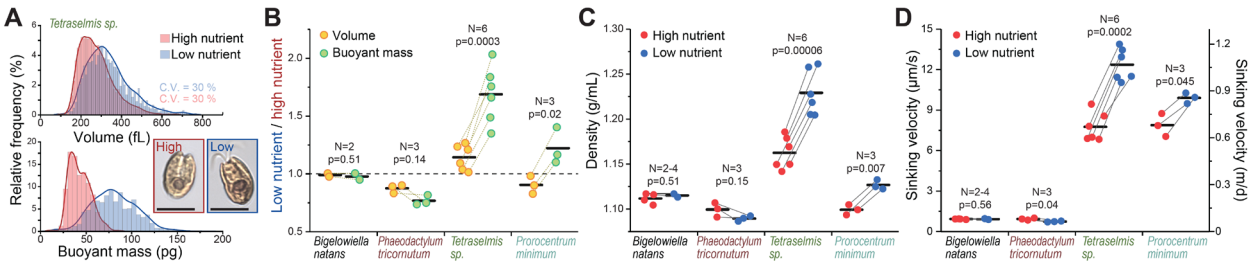

Figure 2. Nutrient limitation increases sinking velocity by increasing cell mass in a species-specific manner.

(A) Single-cell mass and volume histograms for *Tetraselmis sp*. in high (red) and low (blue) nutrients. Inset displays representative images of the cells. Scales bars denote 5 µm. **(B)** Change in cell volume (orange) and buoyant mass (green) between low and high nutrient conditions. **(C-D)** Cell density (C) and sinking velocity (D) in high (red) and low (blue) nutrients.

In (B-D), dots depict independent experiments, N indicates the number of independent experiments, paired samples are connected by a line, and horizontal lines depict mean values. p-values were obtained by pair-sample t-test.

changed more significantly than volume. In *Tetraselmis sp.* and *Prorocentrum minimum* mass increase resulted in increased cell densities (Fig 2C) and significantly increased sinking velocities (Fig 2D). We did not observe any systematic morphological differences between the two nutrient conditions in *Tetraselmis sp.* (Fig 2A).

Next, we wanted to understand if all cells within a given species display similar sinking velocities. We focused on the two species displaying strong nutrient responses, *Prorocentrum minimum* and *Tetraselmis sp.* The former is a globally distributed, bloom-forming dinoflagellate that produces toxins impacting shellfish populations and human health (13). *Tetraselmis sp.* is an industrially relevant green alga with high lipid production capacity and uses in aquaculture (14, 15). To measure intraspecies heterogeneity in cell densities and sinking velocities, we coupled our buoyant mass measurements with fluorescence exclusion-based volume measurements. *Tetraselmis sp.* displayed cell density coefficient of variabilities (CVs) of 2-3% (Fig 3A), which is an order of magnitude more than what is observed in typical eukaryotic model systems (16). Consequently, there is significant cell-to-cell variability in sinking velocities (CV ~20%, Fig 3A). We then correlated cell volumes with sinking velocities. We observed that ~50% of the cell-to-cell variability in sinking velocities was explained by cell volumes (R^2~0.5, Fig 3B). Cell densities did not display volume-dependency and, consequently, the sinking velocities scaled with cell volumes according to the ⅔-power law (Fig 3B). *Prorocentrum minimum* exhibited similar results (Supplemental dataset S7).

Finally, we also examined if *Tetraselmis sp.* displays light-dependency in its sinking velocities under autotrophic conditions. The presence of light had no influence on sinking velocities under high nutrient conditions (Fig 3C). However, light was required for cells to increase sinking velocity under low nutrient conditions (Fig 3C).

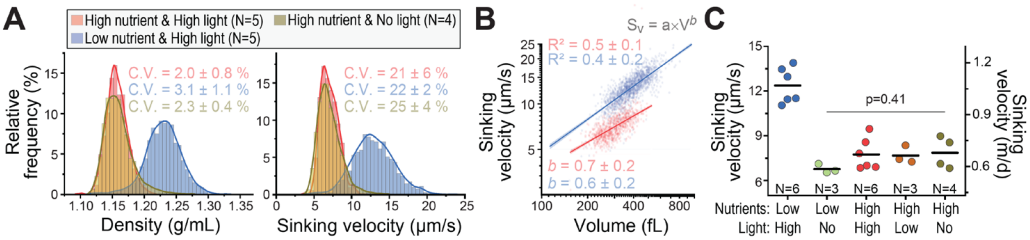

Figure 3. *Tetraselmis sp.* single-cell sinking velocities depend ~50% on cell volume.
(A) Single-cell density and sinking velocity histograms for *Tetraselmis sp*. in indicated conditions. C.V. values (mean±SD) are indicated. **(B)** Correlations between single-cell sinking velocities and volumes for high (red) and low (blue) nutrient conditions. Lines and shaded areas indicate power law fits and their 95% confidence bands, opaque dots depict single cells. Pearson correlation values (R^2) and power law scaling factors (*b*) are indicated as mean±SD. **(C)** Population average sinking velocities under indicated nutrient and light conditions. Dots depict independent experiments, and horizontal lines depict mean values, p-value for comparison of indicated conditions were obtained by ANOVA. N indicates the number of independent experiments.

DISCUSSION

Our results reveal the inter- and intraspecies heterogeneity, as well as selected nutrient responses, in algal sinking velocities. We observed increased sinking velocities in motile algae under nutrient limitations, which may reflect an evolutionary adaptation that allows the algae to sink faster to deeper, nutrient richer waters. Surprisingly, this increase in sinking velocities was achieved by increasing cell mass with minimal changes to cell volume. Larger cell biomass under a nutrient limitation may seem counterintuitive, as cell growth is also limited. However, even under low growth conditions, cell mass can increase if proliferation rate is sufficiently decreased (17, 18), and we verified that *Tetraselmis sp.* stops proliferation in our low

nutrient conditions. The reason why cells adjust their mass but not volume remains unknown, but this could reflect the ecological constraints that cell volume imposes on the algae. For example, predation (grazing and viral infection) and respiration can be impacted by cell volume (19–21), whereas cell mass is less constrained. Notably, we also observed that the mass and sinking velocity increase during nutrient limitation requires light. This finding supports the larger paradigm that uncoupling of photosynthesis and biosynthesis may have important biogeochemical consequences (22, 23).

Our study reveals that gravitational sinking of motile algae can vary significantly depending on the environment. While gravitational sinking could be counteracted by motility, this would come with a significant energetic cost to the cell, with higher mass (and density) cells consuming more energy to counteract sinking. Consequently, it is possible that motile species cannot fully counteract gravitational sinking, and we propose that calculations of carbon sequestration via gravitational sinking should also consider motile species.

Our results also reveal the cell volume dependency of sinking velocities within and between species. Larger cells sink faster than smaller cells, approximately according to ⅔-power law scaling. While this may provide larger cells with an advantage in reaching deeper waters with more nutrients faster than smaller cells, it will also force larger cells to consume more energy to counteract sinking out of the photic zone. These results highlight the need for size homeostasis in algae.

Finally, our work is a proof of methodology that could support marine ecology research and modeling of carbon fluxes. With the development of automated sample preparation methods that separate large algae aggregates from single cells of different sizes, the SMR could be adapted for measurements of algae directly from the ocean. Such future approaches could provide high throughput sinking velocity measurements *in situ*.

MATERIALS AND METHODS

Algal culture conditions

All algae were obtained from Provasoli-Guillard National Center for Marine Algae and Microbiota (NCMA) and belong to the Culture Collection of Marine Phytoplankton (CCMP), except for two coastal seawater isolates (A & B), which were both identified as *Thalassiosira sp.* according to 18s sequencing. Unialgal cultures were grown in filter-sterilized L1 or L1-Si medium, as appropriate for cell type (see table 1). Cultures were maintained on a benchtop at room temperature (20°C), where they received approximately 50 μm/s/m^2 of photosynthetically active radiation (PAR) as measured by a LI-COR LI-250 light meter. Cultures were transferred to fresh media weekly by a 1:10 dilution under a laminar flow hood and were regularly visually monitored for health (color, cell shape and size, purity, and motility when relevant) using an inverted light microscope at 100x magnification.

Table 1. List of species studied, their CCMP ID and culture maintenance medium.

Species	Class	Culture Collection ID	Maintenance Medium
Micromonas pusilla	Mamelliophyceae	CCMP 1545	L1-Si
Pyramimonas parkeae	Prasinophyceae	CCMP 725	L1-Si
Tetraselmis sp.	Chlorophyta	CCMP 908	L1-Si
Chlamydomonas sp.	Chlorophyta	CCMP 235	L1-Si
Rhodomonas salina	Cryptphyta	CCMP 1319	L1-Si
Bigelowiella natans	Chloarachniophyta	CCMP 2755	L1-Si
Nannochloropsis oculata	Eustigmatophyta	CCMP 525	L1-Si
Phaeodactylum tricornatum	Bacillariophyta	CCMP 632	L1
Isolate A (*Thalassiosira sp.*)	Bacillariophyta	N/A	L1
Isolate B (*Thalassiosira sp.*)	Bacillariophyta	N/A	L1

Thalassiosira pseudonana	Bacillariophyta	CCMP 1335	L1
Prorocentrum minimum	Dinophyta	CCMP 1329	L1-Si
Phaeocystis globosa	Prymnesiophyceae	CCMP 629	L1-Si
Emiliania huxleyi	Prymnesiophyceae	CCMP 2090	L1-Si
Emiliania huxleyi	Prymnesiophyceae	RCC 3962	L1-Si
Isochrysis galbana	Prymnesiphyceae	CCMP 1323	L1-Si
Diachronema lutheri	Pavlovophyceae	CCMP 1325	L1-Si

For the nutrient limitation experiments, two types of media were used: Standard L1 or L1-Si for "high nutrient" conditions, and L1/100 or L1-Si/100 for "low nutrient" conditions, in which the phosphorous, nitrate, trace metals, vitamins, and silica (if applicable) were diluted 1/100, while the salinity and pH of the medium remained unchanged. Algal cultures were pre-grown in maintenance medium for 2 days under benchtop light conditions. Cells were pelleted in a benchtop microcentrifuge at 5000 rpm for 10 min. The supernatant was discarded, and cells were washed once in artificial seawater (pH = 8.2) to prevent nutrient carryover. Cultures were transferred to the appropriate medium for cell type and desired nutrient availability by a 1:10 dilution under a laminar flow hood and placed in the appropriate lighting condition for 5 days.

The three lighting conditions used were "low light", benchtop light from nearby window, with 50 $\mu m/s/m^2$ of PAR and day length varying between 9 h and 15.3 h depending on time of year, "no light" in which cultures were incubated at room temperature in a drawer, and "high light" in which cultures were grown with 100 $\mu m/s/m^2$ of PAR from full spectrum LEDs with a day-night cycle of 11h:13h in a temperature-controlled environmental chamber at 18°C.

All data in Figure 1 is from species grown under "low light" and "high nutrient" conditions.

Phylogeny construction and species verification

Purity and identity of all cultures was verified by Sanger sequencing of the V4 – V9 region of the 18S rRNA gene. To amplify the 18S rRNA gene, cells were lysed by three consecutive freeze-thaw cycles and 1 ul of lysate was added to the *New England Biolabs Taq* 5X MasterMix. The V4-V9 region was amplified using 570F [5'-CGG TAA YTC CAG CTC YAV] and EukB [5'-TGA TCC TTC TGC AGG TTC ACC TAC] primers added to a final concentration of 0.2µM each. PCR cycling conditions were according to manufacturer specifications, with an annealing temperature of 52°C and extension time of 60 seconds. Purity of the amplification product was verified by gel electrophoresis and PCR products were sequenced by Sanger sequencing at Azenta Life Sciences. The resulting sequences were searched by blastn against the NCBI nonredundant nucleotide collection to verify identy and purity of each strain.

The phylogeny was built by downloading the closest match full-length 18s sequence for each strain from NCBI, along with a representative of land plants, ameobae, and animals (NCBI accession numbers XR_004853735, AF114438, and M10098, respectively). Sequences were aligned using Mafft (24) v7.407 default parameters, alignments were trimmed using TrimAL (25) v1.2rev59 default parameters, and the tree was inferred using IQ-TREE (26) v1.6.8 with the model TIM2e+I+G4 as selected by the IQTree model finder. The resulting phylogeny was visualized and edited with FigTree (27) v1.4.4.

Cell count, buoyant mass, and volume measurements

Buoyant mass measurements were carried out using a suspended microchannel resonator (SMR). The SMR is a vibrating cantilever with an internal microfluidic channel that allows single cells to travel through the interior of the cantilever. The resonant frequency of the cantilever changes due to the presence of a cell, and this change is proportional to buoyant mass of the cell. The fabrication and details of the operation of SMR are detailed in (10, 28–30). This study used two different sizes of SMRs, one where the cantilever inner cross-section is 8 µm x 8 µm, and one where the cross-section is 15 µm x 20 µm. Algae species with estimated diameter below 6 µm were measured using the smaller SMR, and larger algae species were measured using the larger SMR. For each measurement, an aliquot of cell culture was transferred to

a vial fluidically connected to the SMR. The SMR was pre-filled with cell culture medium to remove any possible changes of culture environment during the measurement. Single cells were flushed through the SMR, and each cell measurement lasted <100 ms (travel time through the cantilever). All measurements were carried out between 10am and 6pm.

Cell volume was measured using a Coulter counter (Multisizer 4, Beckman Coulter), which is based on the principle that a cell traversing an orifice filled with electrolyte will produce an impedance change proportional to the volume of the cell due to displacement of electrolyte. The Coulter counter was pre-filled with cell culture medium before measurement. An aliquot of cell culture was transferred to a cuvette from which the Coulter counter withdrew a fixed volume and monitored single-cell events. Algae cells were measured with one of two Coulter counter apertures, one 20 µm and one 100 µm in diameter, with the selection of aperture depending on the size of the algae cells. Cell counting was also based on coulter counter measurements. Each cell is measured in ~1 ms (travel time through the coulter counter aperture).

For SMR data analysis, the raw data of real-time resonant frequency were analyzed by custom MATLAB code which detects the resonant frequency change caused by passage of a cell (29). The frequency change for each cell was converted to buoyant mass of the cell based on calibration using NIST-certified polystyrene beads (3 µm and 10 µm in diameter, Duke Standards™, Thermo Scientific). For Coulter counter data analysis, the electrical impedance-based cell volumes are automatically available from the Coulter counter and these values were re-calibrated based on measurements of NIST-certified polystyrene beads (2 µm and 6 µm in diameter, Duke Standards™, Thermo Scientific).

Microscopy-based volume and shape measurements

Cell volume and shape were determined by microscopy of unialgal cultures by *EnviroScience, Inc* (OH, USA). Live cultures were shipped overnight from Cambridge, MA to Stow, OH at ambient temperature. Upon arrival, 0.1 mL was places into a Palmer-Maloney nano-plankton counting chamber and allowed to settle. In the case that cells are too motile to acquire clear images, the sample was fixed with 1 drop of Lugol's solution. A microscope-mounted camera was used to acquire images and dimension and volume measurements were acquired by automated image processing software.

Sinking velocity calculations

Algae sinking velocities were calculated according to the Stokes' law (*equation 1*), using the following values for environmental constants in surface ocean: the dynamic viscosity of seawater of 1.07×10^{-3} Pa·s at 20ºC, and density of seawater of 1.02 g/ml. Both high- and low-nutrient culture medias displayed similar densities, as quantified by SMR following a previously reported protocol (11, 31). Cell radius was calculated from cell volume and cell density was calculated using the volume and buoyant mass measurements (*equation 2*). The Stokes' law is a solution to the Navier-Stokes equation at low (<0.5) Reynolds number (*Re*). The Reynolds number for sinking algae is defined as $Re = \rho V_s D/\mu$, where ρ refers to the density of seawater, V_s refers to the sinking velocity and μ refers to the dynamic viscosity of seawater. In all agal species tested in this study, the Reynolds numbers do not exceed the scale of 10^{-7}.

The Stokes' law drag force was also corrected to account for non-spherical cell shapes, The correction was carried out according to previous empirical results for a variety of shapes (9). The shape and aspect ratio for each species were first determined based on microscopic images obtained in this study and/or provided by algae supplier (NCMA). A multiplicative shape factor was calculated for each species based on its shape and aspect ratio. All results shown in figures are without this correction factor, as the calculated corrections were too minor to be clearly visible on the graphs (except for a single species, *Phaeodactylum tricornutum*).

Single-cell density and sinking velocity measurements

Single-cell densities and sinking velocities were obtained by coupling buoyant mass measurements with fluorescence exclusion-based volume measurements (32) within the SMR device by building a fluorescence microscope on top of the SMR. In fluorescence exclusion measurements, the media contains a fluorophore, which is cell impermeable. When the fluorescence signal from a fixed volume is measured

with and without a cell, the signal intensity decreases according to the volume of the cell as fluorescent media is excluded from the measurement volume. In practice, cells were immersed in culture media containing 5 mg/mL Fluorescein isothiocyanate–dextran (Sigma-Aldrich, Cat#FD2000S, molecular weight 2,000,000 g/mol) and flown through the SMR. Immediately after the SMR cantilever, the cells flowed through a fluorescence measurement area where the sample was exited with 482 nm light. Emission from the fluorescent dextran was collected with a photomultiplier tube using 515/30 nm emission filter. A typical measurement duration is 2 ms (time that the cell travels through the fluorescence measurement area).

SMR and fluorescence exclusion measurement data were paired using time information for each cell measurement, with a typical time lag between the two measurements being 10 ms. Cell volume was obtained by calculating the ratio between fluorescence signal decrease when a cell travels through the measurement area and the fluorescence baseline when a cell is not present in the measurement area. These cell volumes were then calibrated to absolute volume units by comparing the population size distributions to those measured with Coulter Counter. Single-cell densities and sinking velocities were calculated from the buoyant mass and volume data as detailed above for population-level measurements.

Data analysis and statistics

In all figures, n refers to the number of single cells measured, while N refers to the number of independent experiments. High and low nutrient conditions under high light were prepared as paired samples (a single cell culture was separated into the two conditions at the beginning of the experiment). The background noise of the measurements was determined using a blank sample (no cells) and particles too small to be viable cells were removed from all final analyses. For single-cell density measurements, particles with density above 1.7 g/mL were excluded, as these were likely due to mispairing of mass and volume measurements. Analyses of allometric scaling were carried out using a power law fit to the single cell data, with each data point weighted equally and without fixing the intercept. All experiments were analyzed independently of each other, and reported errors for power law scaling factors reflect the error between independent experiments. Statistical comparisons used are indicated in the figure legends and comparisons were done using the OriginPro 2023 software.

Data availability

All buoyant mass and volume data, which were used to calculate densities and sinking velocities, are included in the Supplemental datasets S1-S7.

ACKNOWLEDGMENTS

This work was supported by the Simons Foundation (Life Sciences Project Award – 572792) to M.F.P. and S.R.M.

Conflict of interest

S.R.M. is a co-founder of Travera and Affinity Biosensors, which develops techniques relevant to the research presented. The remaining authors declare no competing interests.

Author contributions

T.P.M., A.L.G. and Y.W. designed the research and analyzed the data; T.P.M., A.L.G., Y.W., W.W. and T.R.U. carried out the experiments; B.R.K.R., M.F.P. and S.R.M. provided resources and conceptual feedback; and T.P.M., A.L.G. and Y.W. wrote the paper with input from all authors.

REFERENCES

1. C. B. Field, M. J. Behrenfeld, J. T. Randerson, P. Falkowski, Primary production of the biosphere: Integrating terrestrial and oceanic components. *Science* **281**, 237–240 (1998).
2. K. A. Miklasz, M. W. Denny, Diatom sinkings speeds: Improved predictions and insight from a modified Stokes' law. *Limnol Oceanogr* **55**, 2513–2525 (2010).
3. H. W. Ducklow, D. K. Steinberg, K. O. Buesseler, Upper Ocean Carbon Export and the Biological Pump. *Oceanography* **14**, 50–58 (2001).
4. C. A. Durkin, B. A. S. Van Mooy, S. T. Dyhrman, K. O. Buesseler, Sinking phytoplankton associated with carbon flux in the Atlantic Ocean. *Limnol Oceanogr* **61**, 1172–1187 (2016).
5. S. Dutkiewicz, M. J. Follows, J. G. Bragg, Modeling the coupling of ocean ecology and biogeochemistry. *Global Biogeochem Cycles* **23**, 4017 (2009).
6. J. D. Wilson, *et al.*, The biological carbon pump in CMIP6 models: 21st century trends and uncertainties. *Proc Natl Acad Sci U S A* **119** (2022).
7. B. J. Gemmell, G. Oh, E. J. Buskey, T. A. Villareal, Dynamic sinking behaviour in marine phytoplankton: rapid changes in buoyancy may aid in nutrient uptake. *Proceedings of the Royal Society B: Biological Sciences* **283** (2016).
8. A. E. Walsby, D. P. Holland, Sinking velocities of phytoplankton measured on a stable density gradient by laser scanning. *J R Soc Interface* **3**, 429–439 (2005).
9. D. Leith, Drag on Nonspherical Objects. *Aerosol Science and Technology* **6**, 153–161 (2007).
10. T. P. Burg, *et al.*, Weighing of biomolecules, single cells and single nanoparticles in fluid. *Nature* **446**, 1066–1069 (2007).
11. L. Mu, *et al.*, Mass measurements during lymphocytic leukemia cell polyploidization decouple cell cycle- And cell size-dependent growth. *Proc Natl Acad Sci U S A* **117**, 15659–15665 (2020).
12. N. Cermak, *et al.*, Direct single-cell biomass estimates for marine bacteria via Archimedes' principle. *The ISME Journal 2017 11:3* **11**, 825–828 (2016).
13. C. A. Heil, P. M. Glibert, C. Fan, Prorocentrum minimum (Pavillard) Schiller: A review of a harmful algal bloom species of growing worldwide importance. *Harmful Algae* **4**, 449–470 (2005).
14. M. Alonso, F. C. Lago, J. M. Vieites, M. Espiñeira, Molecular characterization of microalgae used in aquaculture with biotechnology potential. *Aquaculture International* **20**, 847–857 (2012).
15. C. Lauritano, *et al.*, New molecular insights on the response of the green alga Tetraselmis suecica to nitrogen starvation. *Sci Rep* **9** (2019).
16. G. E. Neurohr, A. Amon, Relevance and Regulation of Cell Density. *Trends Cell Biol* **30**, 213–225 (2020).
17. T. P. Miettinen, M. J. Caldez, P. Kaldis, M. Björklund, Cell size control – a mechanism for maintaining fitness and function. *BioEssays* **39** (2017).
18. A. A. Amodeo, J. M. Skotheim, Cell-Size Control. *Cold Spring Harb Perspect Biol* **8**, a019083 (2016).
19. B. C. Monger, M. R. Landry, Prey-size dependency of grazing by free-living marine flagellates*. *Mar Ecol Prog Ser* **74**, 239–248 (1991).
20. A. G. Murray, G. A. Jackson, Viral dynamics: a model of the effects of size, shape, motion and abundance of single-celled planktonic organisms and other particles. *Mar Ecol Prog Ser* **89**, 103–116 (1992).
21. H. Hillebrand, *et al.*, Cell size as driver and sentinel of phytoplankton community structure and functioning. *Funct Ecol* **36**, 276–293 (2022).
22. K. H. Halsey, B. M. Jones, Phytoplankton Strategies for Photosynthetic Energy Allocation. *Ann Rev Mar Sci* **7**, 265–297 (2015).
23. Z. Wu, *et al.*, Modeling Photosynthesis and Exudation in Subtropical Oceans. *Global Biogeochem Cycles* **35**, e2021GB006941 (2021).
24. K. Katoh, D. M. Standley, MAFFT Multiple Sequence Alignment Software Version 7: Improvements in Performance and Usability. *Mol Biol Evol* **30**, 772–780 (2013).

25. S. Capella-Gutiérrez, J. M. Silla-Martínez, T. Gabaldón, trimAl: a tool for automated alignment trimming in large-scale phylogenetic analyses. *Bioinformatics* **25**, 1972–1973 (2009).
26. L. T. Nguyen, H. A. Schmidt, A. Von Haeseler, B. Q. Minh, IQ-TREE: A Fast and Effective Stochastic Algorithm for Estimating Maximum-Likelihood Phylogenies. *Mol Biol Evol* **32**, 268–274 (2015).
27. A. Rambaut, FigTree-version 1.4. 4, a graphical viewer of phylogenetic trees (2018).
28. S. Olcum, *et al.*, Weighing nanoparticles in solution at the attogram scale. *Proc Natl Acad Sci U S A* **111**, 1310–1315 (2014).
29. J. H. Kang, *et al.*, Noninvasive monitoring of single-cell mechanics by acoustic scattering. *Nat Methods* **16**, 263–269 (2019).
30. T. P. Miettinen, K. S. Ly, A. Lam, S. R. Manalis, Single-cell monitoring of dry mass and dry mass density reveals exocytosis of cellular dry contents in mitosis. *Elife* **11** (2022).
31. W. H. Grover, *et al.*, Measuring single-cell density. *Proc Natl Acad Sci U S A* **108**, 10992–10996 (2011).
32. C. Cadart, *et al.*, Fluorescence eXclusion Measurement of volume in live cells. *Methods Cell Biol* **139**, 103–120 (2017).